Advanced-ignition-concept exploration on OMEGA

2009 Plasma Phys. Control. Fusion 51 124052

(http://iopscience.iop.org/0741-3335/51/12/124052)

Plasma Phys. Control. Fusion **51** (2009) 124052 (12pp) doi:10.1088/0741-3335/51/12/124052

Advanced-ignition-concept exploration on OMEGA

W Theobald[1], K S Anderson[1,6], R Betti[1,6,7,8], R S Craxton[1], J A Delettrez[1], J A Frenje[2], V Yu Glebov[1], O V Gotchev[1,6], J H Kelly[1], C K Li[2], A J Mackinnon[3], F J Marshall[1], R L McCrory[1,7,8], D D Meyerhofer[1,6,7,8], J F Myatt[1], P A Norreys[4], P M Nilson[1,6], P K Patel[3], R D Petrasso[2], P B Radha[1], C Ren[1,6,7], T C Sangster[1], W Seka[1], V A Smalyuk[1], A A Solodov[1,6], R B Stephens[5], C Stoeckl[1] and B Yaakobi[1]

[1] Laboratory for Laser Energetics, University of Rochester, Rochester, NY 14623, USA
[2] Massachusetts Institute of Technology, Cambridge, MA 02439, USA
[3] Lawrence Livermore National Laboratory, Livermore, CA 94550, USA
[4] Rutherford Appleton Laboratory, Didcot OX11 0QX, UK
[5] General Atomics, San Diego, CA 91286, USA

E-mail: wthe@lle.rochester.edu

Received 19 June 2009, in final form 7 August 2009
Published 12 November 2009
Online at stacks.iop.org/PPCF/51/124052

Abstract
Advanced ignition concepts, such as fast ignition and shock ignition, are being investigated at the Omega Laser Facility. Integrated fast-ignition experiments with room-temperature re-entrant cone targets have begun, using 18 kJ of 351 nm drive energy to implode empty 40 μm thick CD shells, followed by 1.0 kJ of 1053 nm wavelength, short-pulse energy. Short pulses of 10 ps width have irradiated the inside of a hollow gold re-entrant cone at the time of peak compression. A threefold increase in the time-integrated, 2 to 7 keV x-ray emission was observed with x-ray pinhole cameras, indicating that energy is coupled from the short-pulse laser into the core by fast electrons. In shock-ignition experiments, spherical plastic-shell targets were compressed to high areal densities on a low adiabat, and a strong shock wave was sent into the converging, compressed capsule. In one experiment, 60 beams were used with an intensity spike at the end of the laser pulse, and the implosion performance was studied through neutron-yield and areal-density measurements. In a second experiment, the 60 OMEGA beams were split into a 40 + 20 configuration, with

[6] Also at: Fusion Science Center for Extreme States of Matter and Fast Ignition Physics, University of Rochester, Rochester, NY, USA.
[7] Also at: Mechanical Engineering Department, University of Rochester, Rochester, NY, USA.
[8] Also at: Physics Department, University of Rochester, Rochester, NY, USA.

40 low-intensity beams used for fuel assembly and 20 delayed beams with a short, high-intensity pulse shape (up to 1×10^{16} W cm^{-2}) for shock generation.

1. Introduction

Shock ignition [1] (SI) and fast ignition [2, 3] (FI) are attractive options for inertial confinement fusion (ICF). These two-step ICF processes separate fuel assembly and ignition, relaxing the driver requirements and promising high gains [1, 4]. The cone-in-shell concept [5] is of significant current interest for FI because of promising initial integrated experiments [6, 7]. The reentrant cone makes it possible for a high-energy petawatt laser (HEPW) pulse to propagate as close as possible to the dense core, avoiding the need to transport through a large region of plasma. The HEPW laser creates an intense, suprathermal electron current at the critical-density surface inside the hollow cone. Most of the accelerated electrons have a momentum directed toward the compressed core. In an ignition design, the megaelectronvolt electrons must deposit several tens of kilojoules of energy into the compressed core [8, 9]. Many unresolved issues remain in the physics of fast-electron generation with HEPW lasers. These issues include the laser-to-electron-conversion efficiency [10], the fast-electron-energy spectrum [11] and the dynamics of the high-current propagation from the critical-density surface through the high-Z cone-wall material [12] and from the cone tip into the assembled fuel [13]. Along the megaelectronvolt-electron paths, the background plasma electron densities vary by more than four orders of magnitude and the temperatures vary from ~1 eV to several kiloelectronvolts [14].

Integrated FI experiments with a re-entrant cone were performed at Osaka University with up to 2.6 kJ of long-pulse laser energy and ~300 J of short-pulse laser energy (0.5 PW, 0.5 ps). The experiments clearly demonstrated that there is significant heating induced by the short pulse [7]. The Omega [15]/Omega EP [16] Laser Facility is beginning to perform integrated FI experiments that use drive-laser and short-pulse-laser energies of ~18 kJ and 1 kJ, respectively. Shaped laser pulses are optimized for achieving FI-relevant high areal densities [17].

SI is a two-step ICF concept in which a strong spherically convergent shock wave is launched at the end of the laser pulse to ignite the compressed core of a low-velocity implosion [1, 18, 19]. SI has the advantage of reducing the energy required for ignition using a single laser system, unlike FI [2], which requires two separate laser systems. Proof-of-principle experiments [1] could be carried out on the National Ignition Facility [20]. The spherically convergent shock wave (ignitor shock) propagates through the shell during the coasting phase of the implosion. This ignitor shock is launched at the end of the laser pulse by a spike with intensity in the range from 3×10^{15} to 10^{16} W cm^{-2}. It collides with the return shock near the inner shell surface. After the ignitor and return shock collide, a third shock wave propagates inward, leading to further compression of the hot spot. The final fuel assembly develops a centrally peaked pressure profile. Such non-isobaric assemblies exhibit a lower ignition threshold than standard isobaric ones [1].

This paper describes the recent investigations of the physics of the FI and SI concepts at LLE. Initial integrated FI experiments with re-entrant cone targets using 18 kJ drive energy and short-pulse energies of up to 1.0 kJ are described in section 2. Section 3 describes SI experiments that employ both 60-beam spherical implosions and a configuration using 40 beams for fuel assembly and 20 delayed, tightly focused beams for shock generation. Section 4 provides a short summary.

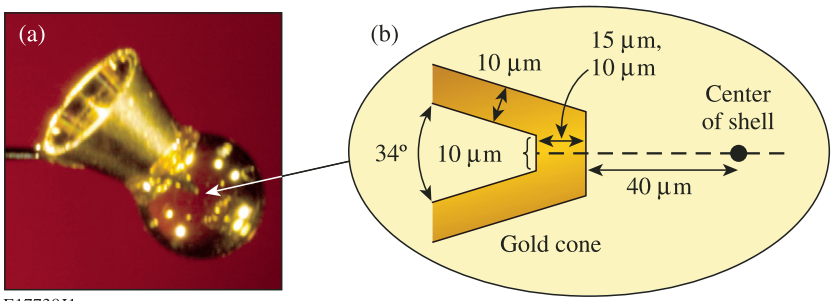

Figure 1. (*a*) Photograph of a gold re-entrant cone target; (*b*) schematic showing the cone-tip dimensions.

2. Integrated FI experiments

Integrated FI experiments have begun at the Omega [15]/Omega EP [16] Laser Facility. The targets are 40 μm thick empty CD shells of ~870 μm outer diameter, where a hollow gold cone with a full opening angle of 34° is inserted through a hole in the shell (see figure 1). The cone has a side-wall thickness of 10 μm with 10 and 15 μm thick tips. A low-adiabat ($\alpha = 1.5$) laser pulse comprised a short picket pulse and a shaped ~2.7 ns drive pulse with 351 nm wavelength and ~18 kJ of energy imploded the capsule [17]. The adiabat α is defined as the ratio of the plasma pressure to the Fermi pressure of a degenerate electron gas [21]. OMEGA implosions have demonstrated an average areal density $\langle \rho R \rangle = 0.22\,\mathrm{g\,cm^{-2}}$ and peak areal densities $(\rho R)_{\max} > 0.3\,\mathrm{g\,cm^{-2}}$ in a spherical surrogate-CH target filled with 8 atm of D_2 gas using a similar laser pulse shape [22]. Even higher areal densities are expected with an empty shell. In the cone geometry the ρR is typically ~60% of that achieved in spherically irradiated targets [23]. Two-dimensional hydrodynamic simulations using the code *DRACO* [24] are in qualitative agreement with experimental hydrodynamic studies of direct-drive cone-in-shell targets [23, 25, 26]. The assembled areal densities are sufficient to stop up to 2 MeV electrons in compressed plastic shells. In an ignition target, electrons with ~1.5 MeV energy have a stopping range of $1.2\,\mathrm{g\,cm^{-2}}$ in $300\,\mathrm{g\,cm^{-3}}$ DT fuel. Therefore, megaelectronvolt electrons with energies that are relevant for a DT ignition target design can be stopped in surrogate implosions on OMEGA. The 1053 nm wavelength short pulse had an energy of 1 kJ and a duration of 10 ps, and was focused to a spot of ~50 μm diameter containing 80% of the laser energy [27]. The corresponding peak laser intensity at the center of the tip of the cone is estimated to be $\sim 8 \times 10^{18}\,\mathrm{W\,cm^{-2}}$.

In preparation for integrated FI experiments, the short-pulse laser was precisely timed with respect to the drive laser and pointed into the cone tip. The pointing was monitored with x-ray pinhole cameras measuring the emission from a reference implosion and from dedicated pointing shots. The accuracy of pointing for the short-pulse laser was ~20 μm. The timing was measured *in situ* with ±50 ps precision at full energy by operating the nuclear temporal diagnostic [28] in hard x-ray mode. Figure 2 shows time-resolved measurements of the drive-laser pulse shape and the hard x-ray emission generated by the interaction with a FI cone target. The HEPW pulse was timed to a delay of 3.50 ± 0.05 ns with respect to the start of the drive pulse shape (time zero). Two-dimensional radiation-hydrodynamics simulations using *DRACO* [24] predict peak compression at 3.5 ns for these targets. Shock-breakout measurements confirmed that the targets make possible a plasma-free path for the short-pulse laser up to peak compression [25, 26].

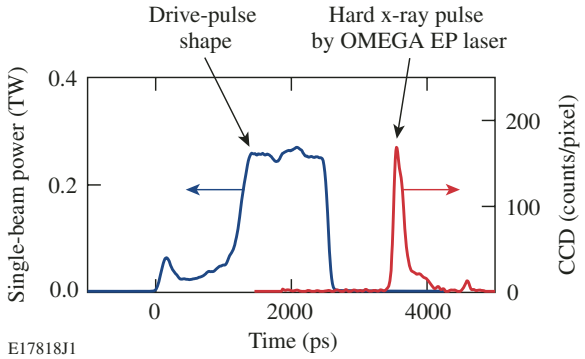

Figure 2. Measured time-resolved hard x-ray emission from an integrated FI experiment.

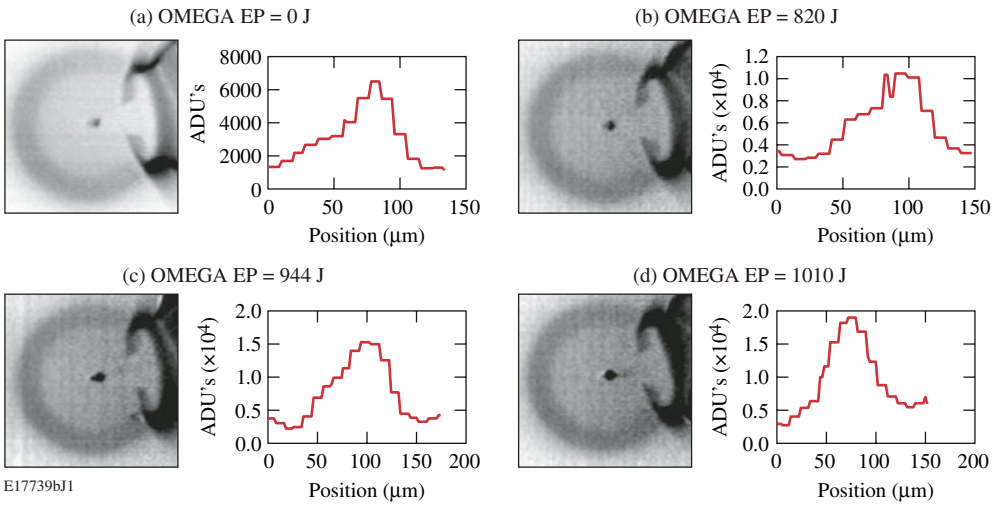

Figure 3. Time-integrated x-ray emission of the heated core region of cone-in-shell targets. The emission is from a photon-energy range from 2 to 7 keV. The short pulse was injected at $t = 3.5$ ns, which is close to the time of peak compression of the imploded shell. The emission is shown in (*a*) without short pulse and in (*b*)–(*d*) for various short-pulse energies.

Figure 3 shows time-integrated x-ray emission pictures from a pinhole camera. Adjacent to each picture is a lineout that was taken through the center portion of the hot plasma region. Figure 3(*a*) shows the emission without the short pulse and figures 3(*b*)–(*d*) with the short pulse. The emission from the gold cone tip is slightly higher than from the core. The images clearly show a significant increase in emission with higher short-pulse energy. At short-pulse energies exceeding ∼1 kJ, the emission from the compressed core and the cone tip is about a factor of 3 higher compared with similar implosions without a short-pulse beam. This indicates that at higher short-pulse laser energies, fast-electron energy is coupled into the compressed shell. The pinhole images provide, however, only qualitative information. Yield measurements of the 2.45 MeV neutrons from D–D fusion reactions are required to obtain quantitative information on the coupling efficiency.

Neutron-yield measurements were attempted in this experiment, but were challenging because of the emission of an intense γ-ray pulse. The strong background consisted of

bremsstrahlung emission generated by megaelectronvolt electrons streaming through the gold cone target. The neutron time-of-flight (nTOF) detectors were appropriately shielded with a ∼25 mm lead housing and the microchannel plate detector was gated to reduce the x-ray and γ-ray fluence [29, 30]. The γ-ray pulse induced a fluorescence background that persisted for several hundred nanoseconds and masked the much weaker neutron signal. Further detector development will be pursued to obtain reliable neutron-yield measurements for the integrated FI experiments. Scintillators with fast light-decay characteristics and very low afterglow are required for these measurements. Organic liquid scintillators that are saturated with molecular oxygen show very promising properties. Fluorescence measurements with γ rays show a significant reduction in afterglow compared with standard organic scintillators without a quenching agent [31].

To simulate the integrated FI experiments on OMEGA/OMEGA EP [13, 32], the 2D radiation-hydrodynamics code *DRACO* [24] in cylindrical geometry has been coupled with the 2D/3D implicit hybrid particle-in-cell code *LSP* [33]. *LSP* provides an implicit solution for the electromagnetic fields and an implicit particle push and is used to simulate the transport of hot electrons in the dense plasmas and heating of the dense fuel. This provides an additional source term in the temperature equations in *DRACO*. The plasma profiles in *LSP* are periodically updated according to the *DRACO* results. *DRACO* simulates the implosion dynamics close to the time of maximum areal density of the compressed shell. With the onset of the short-pulse laser, *LSP* starts calculating the fast-electron beam transport and heating in the target. *LSP* runs for periods of time when the hydrodynamic expansion of the plasma is negligible (∼1 ps) and generates a time history of hot-electron deposition that is used as an energy source in the temperature equation in *DRACO*. *DRACO* runs for the same time interval and updates the hydrodynamic plasma parameters. *DRACO* and *LSP* run together for the duration of the short-pulse interaction, while *DRACO* alone simulates the hydrodynamic response of the target after the short-pulse laser ceases. The short-pulse laser–plasma interaction was not simulated in detail with *LSP*. A simplified model was used to generate a fast-electron beam in the laser's forward direction by promoting background electrons to higher energies using ponderomotive scaling [34] for a given laser intensity (5×10^{19} W cm^{-2}) and a constant conversion efficiency (assumed 30%) of laser energy into fast electrons. A hot-electron beam with a square temporal profile and a Gaussian radial profile (20 μm full width at half maximum (FWHM)) was generated with a relativistic Maxwellian hot-electron-energy distribution function with a characteristic energy of 1.2 MeV. The electrons were injected 70 μm away from the target center with a beam angular spread of 40° FWHM.

Figure 4(*a*) shows a 2D map of the plasma temperature increase from a simulation [32] with a short pulse of 2.6 kJ energy and 10 ps duration. Suprathermal electrons strongly heat the target so that the temperature increases by up to ∼1 keV in some parts of the dense shell. The simulations show that the fast electrons are well collimated by self-generated resistive magnetic fields despite a high initial beam divergence [32]. Figure 4(*b*) shows the predicted neutron yield produced through fast-electron heating as a function of the short-pulse energy. Simulations were performed for various experimental conditions. A conversion efficiency of 30% from short-pulse energy into fast electrons was assumed for the triangle symbols, while 20% was assumed for the diamonds and the circle. Conversion efficiencies of 20 ± 10% of laser energy into suprathermal electrons were measured from flat Cu foil targets under similar experimental conditions [35]. A neutron yield of up to 3×10^9 is predicted for 2.6 kJ with a 20 μm focus and a 10 ps pulse duration. The circle (blue) shows the calculated yield for 1 ps and 0.5 kJ. On OMEGA EP, the short-pulse laser energy is limited to ∼0.5 kJ at ∼1 ps duration, while higher laser energies are available at longer durations. Figure 4(*b*) shows that the neutron yield increases significantly with laser energy. The predicted yield is optimistic

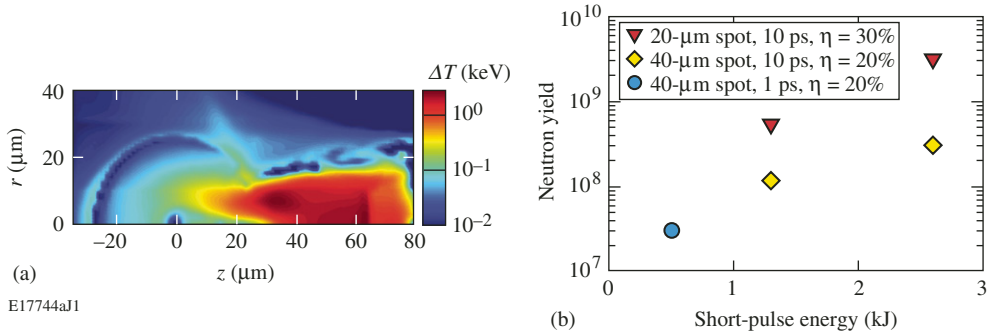

Figure 4. (*a*) Predicted increase in plasma temperature caused by fast-electron heating for 2.6 kJ of short-pulse energy in 10 ps and (*b*) calculations of neutron yield produced through fast-electron heating versus short-pulse energy for various experimental conditions.

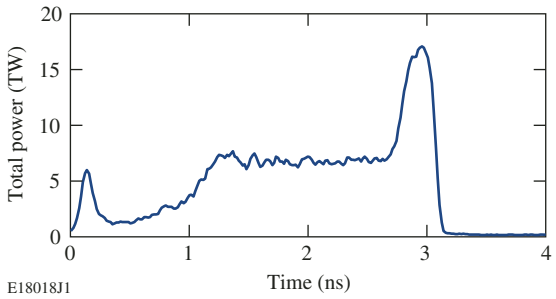

Figure 5. Optimized SI laser-pulse shape that was used to implode D_2-filled, 40 μm plastic shells. The graph shows the laser power of all 60 OMEGA beams versus times.

because the transport through the gold cone was not included in the simulations. Fast-electron transport through the tip of the gold cone is significantly affected by the material properties and will affect the neutron yield.

3. Shock-ignition experiments

Shock-ignition experiments [22] were carried out at the Omega Laser Facility [15] to study fuel assembly using 60-beam, low-adiabat, low-velocity symmetric implosions. The experiments used 18 kJ of UV laser energy and 40 μm thick, 870 μm diameter plastic shells coated outside with a 0.1 μm layer of aluminum and filled with deuterium gas of various pressures. The primary purpose of the Al coating is to retain the gas in the capsule. A shock wave was launched by a spike in the laser power at the end of the pulse. The maximum intensity on target during the late power spike was $\sim 8 \times 10^{14}$ W cm^{-2}. These experiments showed a significant improvement in the performance of these implosions compared with conventional implosions without a late spike. Figure 5 shows the optimized SI pulse shape that was obtained in a series of implosions by measuring the neutron yield and areal density (ρR) as a function of the timing of the picket and spike pulses [22]. Shock-wave timing increased the neutron yield by a factor of $\sim$3 and improved ρR by $\sim$20%. The measured laser-energy-absorption was $85 \pm 2\%$, while the predicted value of 90% is slightly higher.

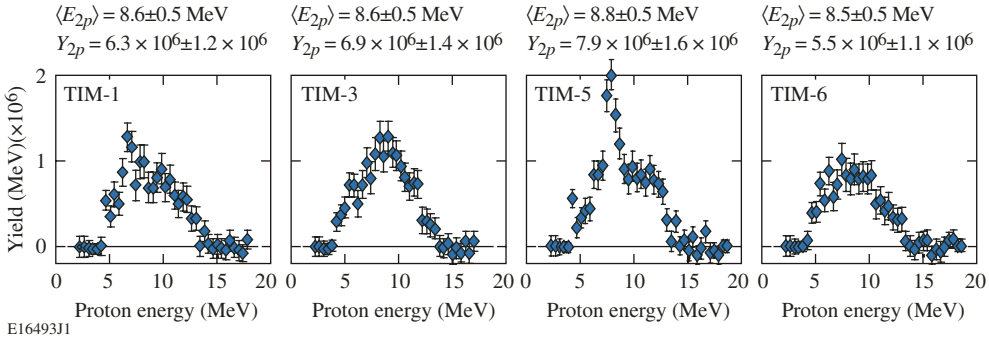

Figure 6. Measured secondary-proton spectra along four different lines of sight for a SI implosion (shot 48674, 18.0 kJ, 8.3 atm of D_2). Very little variation is observed both in the shape of the spectra and in the mean proton energy, indicating a stable implosion.

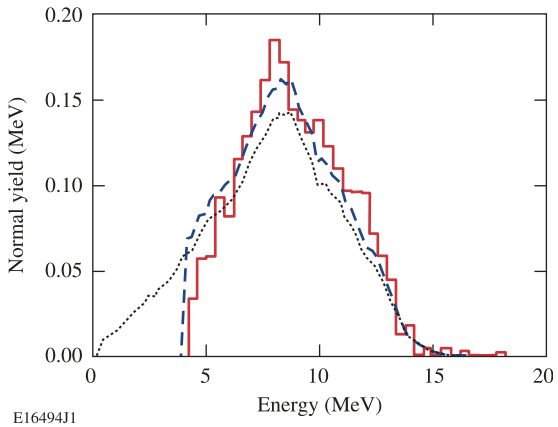

Figure 7. Spatially averaged measured secondary-proton spectrum of a SI implosion (solid), calculated proton spectrum (dotted), and calculated spectrum taking the instrumental cutoff into account (dashed).

Figure 6 shows measured secondary-proton spectra along four different lines of sight for a SI implosion with the optimized pulse shape. Wedged range filters [35] measured the kinetic energy of the protons generated by D^3He fusion reactions—a secondary-proton production reaction in the D_2 fuel. The protons with a birth kinetic energy between 17.5 and 21.6 MeV are downshifted in energy when passing through the cold shell material, enabling the areal density to be inferred. There is very little variation in both the shape of the spectra and the mean proton energy, indicating high shell stability and no significant low-mode variations. A mean proton energy of 8.6 ± 0.15 MeV was measured, corresponding to a mean downshift of 6.4 ± 0.15 MeV. The error bars represent the standard deviation over the four measurements.

All proton spectra are cut off at ~4.5 MeV because of an instrumental effect [36]. Averaging the proton spectra over the different lines of sight results in a mean spectrum that is shown as the solid curve in figure 7. The proton spectrum is sensitive to the proton-production history with respect to the temporal evolution of the areal density [22]. The neutron production rate was measured with the nuclear temporal diagnostic [28] and compared with calculations with the 1D hydrodynamic simulation code *LILAC* [37]. The areal density increases during

neutron production, and the fusion reactions are quenched near the time of peak areal density of $0.33\,\mathrm{g\,cm^{-2}}$, probably caused by mixing cold plastic-shell material into the hot central plasma.

Each point in the time-integrated proton spectrum corresponded to a different downshift and, therefore, sampled a different ρR. The energy downshift of the low-energy tail of the spectrum represents a measure of the peak ρR during the neutron production, which was limited by the instrument indicating $(\rho R)_{\max} > 0.30\,\mathrm{g\,cm^{-2}}$, in agreement with the simulations [22]. The truncation in fusion production close to peak areal density leads to fewer low-energy protons than simulated, which needs to be taken into account when inferring the areal density from the proton spectrum. A downshifted secondary-proton spectrum was calculated with a Monte Carlo code using the ρR evolution and the measured production rate of the fusion reactions [38]. This is shown as the dotted curve in figure 7. A significant portion of the low-energy protons was not detected. The dashed curve takes the instrumental cutoff in the simulated proton spectrum into account and is in very good agreement with the measured secondary-proton spectrum. This agreement shows that a neutron-averaged $\langle \rho R \rangle$ of $0.220 \pm 0.015\,\mathrm{g\,cm^{-2}}$ has been achieved. Without correcting for the cutoff, the instrument gives an $\sim$10% lower $\langle \rho R \rangle$ value than was actually achieved. SI implosions have led to the highest areal density ever measured on OMEGA.

The neutron yield-over-clean (YOC), which is the ratio of measured primary to 1D predicted neutron yield, is typically in the range from 1% to 10% for these low-adiabat implosions. This is caused by mixing cold plastic-shell material into the hot plasma that quenches the fusion reactions. A series of plastic-shell implosions with D_2-fill pressures in the range from 4 to 45 atm were performed [22]. The YOC was measured for implosions with and without a late laser spike as a function of the calculated hot-spot convergence ratio (CR) [22]. The CR is defined as the initial inner-target-shell radius divided by the minimum radius of the gas–shell interface at peak compression. For implosions without a late spike, the YOC drops significantly with increasing CR from $\sim$5% to below 1% for CR = 9 to 23. In comparison, SI-type pulse shapes considerably improve the performance, showing a YOC close to 10% with CRs up to 30. This is attributed to improved shell stability in SI implosions, which might be due to a mitigation of the Rayleigh–Taylor instability at stagnation time using SI-type pulse shapes [19].

The SI implosions also show a significant improvement in $\langle \rho R \rangle$ [22]. On an average, $\langle \rho R \rangle$ is $\sim$30% higher for the SI implosions compared with standard implosions. The areal density observed with warm plastic targets is close to 1D simulation predictions for the SI case [22].

Parametric plasma instabilities [39] such as stimulated Brillouin scattering (SBS), stimulated Raman scattering (SRS) and the two-plasmon-decay (TPD) instability, are of concern in an ignition target design with spike-pulse intensities in the range from 10^{15} to $10^{16}\,\mathrm{W\,cm^{-2}}$ and pulse durations of approximately several hundred picoseconds. The instabilities degrade the laser energy coupling to the capsule. SRS and TPD increase the fraction of the laser energy transferred to hot electrons, which is a potential source of preheat that can reduce the final core compression in functional ICF implosions. In contrast to conventional hot-spot ignition, low-energy hot electrons generated during the power spike may have a positive effect on the implosions for SI [40]. The areal density increases rapidly during the final stages of the implosion. If the range of the hot electrons generated during the spike is less than the shell thickness, they are stopped in the shell and augment the hydrodynamically driven shock wave. The effect of hot electrons on a NIF-scale SI target [40] was modeled in 1D for a marginal igniting target using a multigroup diffusion model [37] for the hot electrons. The shock-launching-time ignition window is considerably wider when the effects of moderate-energy hot electrons (a NIF-scale target can efficiently stop up to 150 keV electrons) are included,

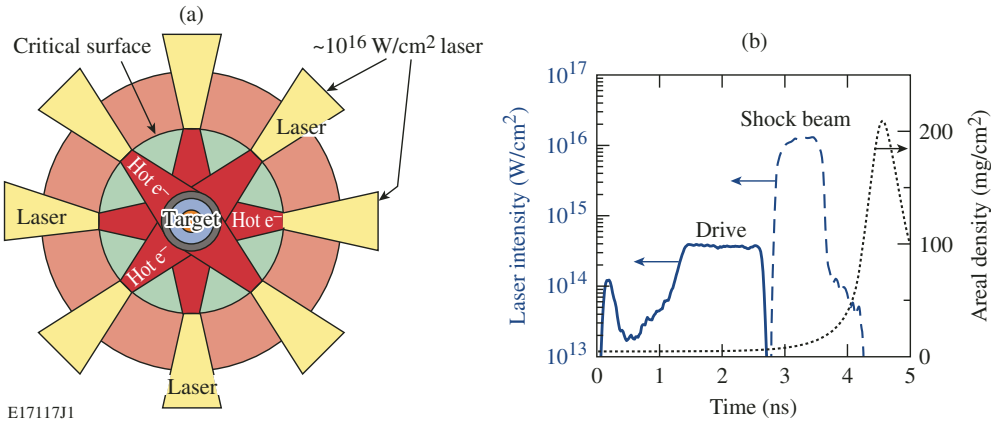

Figure 8. (*a*) Schematic of the setup for studying laser–plasma interactions and preheating at high laser intensities relevant to SI. Forty of the OMEGA laser beams implode the capsule at low intensities. Twenty delayed beams are tightly focused onto the critical-density surface, where plasma instabilities lead to the generation of energetic electrons. Some of them will stream into the dense core. (*b*) Pulse shapes of the 40 drive beams (solid), 20 shock beams (dashed), and areal-density evolution (dotted).

showing that hot electrons may be beneficial for the SI scheme as long as their range is less than the shell thickness.

To test the effect of laser–plasma instabilities and hot electrons, SI laser–plasma experiments have been performed on the OMEGA laser with shock-generating laser intensities of up to $\sim 1 \times 10^{16}\,\mathrm{W\,cm^{-2}}$ [41]. Figure 8 shows a schematic of the experiments. The compression pulse consists of a shaped low-adiabat ($\alpha \sim 1.5$) pulse shape (solid) using 40 OMEGA beams with ~13.6 kJ of UV laser energy. The targets were 36 μm thick, 430 μm outer-radius, deuterated plastic shells coated outside with a 0.1 μm layer of aluminum and filled with D_2 gas with a pressure of ~30 atm. The 351 nm wavelength laser light of the 40 beams was smoothed with polarization smoothing [42] and distributed phase plates [43]. The drive beams had a focal-spot diameter of ~700 μm resulting in a peak intensity of $\sim 3 \times 10^{14}\,\mathrm{W\,cm^{-2}}$. A late shock was driven by the remaining 20 UV beams that were delayed and tightly focused on the compressed core to achieve intensities at the critical-density surface ranging from $\sim 2 \times 10^{15}$ to $\sim 1 \times 10^{16}\,\mathrm{W\,cm^{-2}}$. The intensity was varied by shifting the focus of the 20 shock-driving beams relative to the shell's center and the critical-density surface, respectively. Plasma instabilities in regions of up to quarter-critical density led to the generation of energetic electrons. Some of the fast electrons streamed into the hot core and heated it. The 20 delayed beams (~4.6 kJ) used a ~600 ps FWHM square pulse shape (dashed curve in figure 8(*b*)) that was tightly focused on the shell without polarization smoothing or phase plates. The dotted curve shows the calculated evolution of the areal density.

The illumination configuration for the 40 drive beams was not optimal, with a power imbalance of ~10.6% given as the root-mean-square variation of the laser power on target. In comparison, a typical value of power imbalance for a 60-beam symmetrical illumination on a spherical target is ~2% [44]. Implosion nonuniformity was observed in x-ray-pinhole-camera images that show a strongly perturbed core with a 40-beam implosion. The core distortion was reduced when the delayed 20 tightly focused beams were coupled into the target [41].

The effect of the high-intensity shock beams on neutron and hard x-ray yields was studied as a function of the delay between the 40 and 20 beams (figures 9(*a*) and (*b*)). The delay time

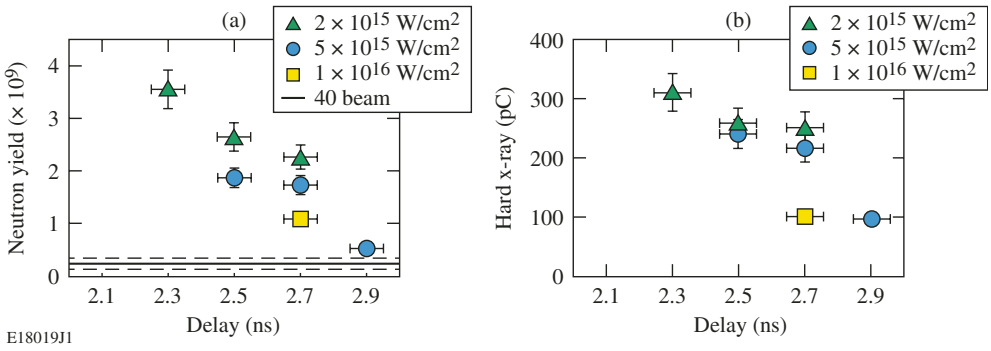

Figure 9. Measured neutron yield (*a*) and hard x-ray yield (*b*) versus the delay time of the high-intensity beam. The different symbols represent different focus positions with respect to the critical-density surface. The solid line in (*a*) is the average yield for 40-beam implosions; the dashed lines represent the error range. The 40-beam implosions produced no measurable hard x-ray signal.

defined by the onset of the high-intensity beam with respect to the start of the drive pulse was varied from 2.3 to 2.9 ns. The symbols correspond to various focus conditions. The legend refers to the estimated vacuum focus intensity at the location of the critical-density surface. Figure 9(*b*) shows the hard x-ray signal, which is indicative of the production of hot electrons. The neutron yield increased by a factor of ∼7 from 5×10^8 to $\sim 3.5 \times 10^9$ for the shortest time delay. A similar trend is observed for the hard x-ray yield, showing a larger amount of hot electrons generated at shorter time delays. Two reference implosions with only 40 drive beams produced neutron yields of 1.4×10^8 and 3.7×10^8; the solid line in figure 9(*a*) represents the average of these yields. The measured neutron yields of the 40-beam implosion show that, despite large target-illumination nonuniformity, a significant amount of the high-intensity-pulse energy is coupled into the capsule, producing up to ∼20× more neutrons and a strong hard x-ray signal.

4. Summary

Advanced ignition concepts such as FI and SI are being investigated on the Omega Laser Facility. Initial integrated fast-ignition experiments with room-temperature re-entrant cone targets were performed using 18 kJ of drive energy to implode empty, 40 μm thick CD shells followed by 1.0 kJ of 10 ps short-pulse energy interacting with a hollow gold re-entrant cone at the time of peak compression. A threefold increase in the time-integrated x-ray emission was observed, indicating that energy is coupled from the short-pulse laser into the core by fast electrons. Neutron detectors were strongly affected by the emission of an intense γ-ray pulse leading to a strong background signal that masks the much weaker neutron signal. Extensive integrated simulations of cone-in-shell fast-ignition targets have been performed, including the implosion and electron transport predicting a significant increase in neutron production with higher short-pulse energy.

In shock-ignition experiments, spherical warm-plastic-shell targets were compressed to high areal densities on a low adiabat, and a strong shock wave was sent into the converging, compressed capsule. Two configurations were studied: first, 60-beam implosions with an intensity spike at the end of the laser pulse were used to study fuel assembly relevant to SI. It was demonstrated that the fuel assembly was close to 1D simulation predictions with averaged

areal densities of 0.22 g cm^{-2} and measured neutron yields that were ∼10% of the 1D predicted yields for a hot-spot CR of ∼30. The shock-ignition implosions measure significantly improved neutron yields and areal densities compared with similar low-adiabat implosions without a spike pulse. Second, the 60 OMEGA beams were split into a 40 + 20 configuration, using 40 low-intensity beams for fuel assembly and 20 delayed beams with a short, high-intensity pulse shape (up to 1×10^{16} W cm^{-2}) for shock generation. The additional 20 high-intensity beams enhanced the neutron yields by a factor of up to ∼20, indicating good coupling of the shock-beam energy to the core.

Acknowledgment

The authors are indebted to the Target Fabrication Groups at General Atomics and LLE. This work was supported by the US Department of Energy Office of Inertial Confinement Fusion under Cooperative Agreement No DE-FC52-08NA28302, the Fusion Science Center No DE-FC02-04ER54789, the OFES ACE FI grant No DE-FG02-05ER54839, the University of Rochester and the New York State Energy Research and Development Authority. The support of DOE does not constitute an endorsement by DOE of the views expressed in this paper.

References

[1] Betti R *et al* 2007 *Phys. Rev. Lett.* **98** 155001
[2] Tabak M *et al* 1994 *Phys. Plasmas* **1** 1626
[3] Basov N G, Gus'kov S Y and Feokistov L P 1992 *J. Sov. Laser Res.* **13** 396
[4] McCrory R L *et al* 2008 *Phys. Plasmas* **15** 055503
[5] Norreys P A *et al* 2000 *Phys. Plasmas* **7** 3721
[6] Kodama R *et al* 2001 *Nature* **412** 798
[7] Kodama R *et al* 2002 *Nature* **418** 933
[8] Atzeni S 1999 *Phys. Plasmas* **6** 3316
[9] Betti R, Solodov A A, Delettrez J A and Zhou C 2006 *Phys. Plasmas* **13** 100703
[10] Kemp A J, Sentoku Y and Tabak M 2008 *Phys. Rev. Lett.* **101** 075004
[11] Haines M G, Wei M S, Beg F N and Stephens R B 2009 *Phys. Rev. Lett.* **102** 045008
[12] King J A *et al* 2009 *Phys. Plasmas* **16** 020701
[13] Solodov A A *et al* 2008 *Phys. Plasmas* **15** 112702
[14] Mason R J 2006 *Phys. Rev. Lett.* **96** 035001
[15] Boehly T R *et al* 1997 *Opt. Commun.* **133** 495
[16] Waxer L J *et al* 2005 *Opt. Photon. News* **16** 30
[17] Zhou C D *et al* 2007 *Phys. Rev. Lett.* **98** 025004
[18] Betti R and Zhou C 2005 *Phys. Plasmas* **12** 110702
[19] Ribeyre X *et al* 2008 *Plasma Phys. Control. Fusion* **50** 025007
[20] Moses E I 2008 *J. Phys. Conf. Ser.* **112** 012003
[21] Zhou C D and Betti R 2007 *Phys. Plasmas* **14** 072703
[22] Theobald W *et al* 2008 *Phys. Plasmas* **15** 056306
[23] Stoeckl C *et al* 2005 *Plasma Phys. Control. Fusion* **47** B856
[24] Radha P B *et al* 2005 *Phys. Plasmas* **12** 056307
[25] Stoeckl C *et al* 2007 *Phys. Plasmas* **14** 112702
[26] Stoeckl C *et al* 2008 *Plasma Phys. Control. Fusion* **50** 124044
[27] Bromage J *et al* 2008 *Opt. Express* **21** 16
[28] Lerche R A, Phillion D W and Tietbohl G L 1995 *Rev. Sci. Instrum.* **66** 933
[29] Glebov V Y *et al* 2004 *Rev. Sci. Instrum.* **75** 3559
[30] Ali Z A *et al* 2008 *Rev. Sci. Instrum.* **79** 10E527
[31] Lauck R *et al* 2009 Low-afterglow, high-refractive-index liquid scintillators for fast-neutron spectrometry and imaging applications *IEEE Trans. Nucl. Sci.* submitted
[32] Solodov A A *et al* 2009 *Phys. Plasmas* **16** 056309

[33] Welch D R, Rose D V, Oliver B V and Clark R E 2001 *Nucl. Instrum. Methods Phys. Res.* A **464** 134
[34] Wilks S C and Kruer W L 1997 *IEEE J. Quantum Electron.* **33** 1954
[35] Nilson P M *et al* 2009 Effect of laser energy and pulse duration on energetic-electron production in Intense laser–solid interactions *Phys. Rev. Lett.* submitted
[36] Séguin F H *et al* 2003 *Rev. Sci. Instrum.* **74** 975
[37] Delettrez J *et al* 1987 *Phys. Rev.* A **36** 3926
Richardson M C *et al* 1986 *Laser Interaction and Related Plasma Phenomena* ed H Hora and G H Miley (New York: Plenum) vol 7 p 421
[38] Radha P B *et al* 2006 *Bull. Am. Phys. Soc.* **51** 106
[39] Kruer W L 1988 The physics of laserplasma interactions *Frontiers in Physics* vol 73 ed D Pines (Redwood City, CA: Addison-Wesley)
[40] Betti R *et al* 2007 *J. Phys. Conf. Ser.* **112** 022024
[41] Theobald W *et al* 2009 Shock-ignition experiments on OMEGA at NIF-relevant intensities *Phys. Rev. Lett.* submitted
[42] Boehly T R *et al* 1999 *J. Appl. Phys.* **85** 3444
[43] Lin Y, Kessler T J and Lawrence G N 1996 *Opt. Lett.* **21** 1703
[44] Marshall F J *et al* 2004 *Phys. Plasmas* **11** 251